JOURNAL OF AIRCRAFT
Vol. 47, No. 5, September–October 2010

Engineering Notes

Analysis of Leading-Edge Separation Bubbles on Rotating Blades

Horia Dumitrescu* and Vladimir Cardoş*
Institute of Statistical Mathematics and Applied Mathematics, Bucharest 050711, Romania

DOI: 10.2514/1.C000274

I. Introduction

THE regions of separated flow that form on blades govern the blade stall characteristics and the loading of wind turbine blades. The nature and extent of these regions are determined primarily (except for the airfoil shape, incidence, and Reynolds number) by the two most important parameters that trigger three-dimensional (3-D) effects, and they are the radius by chord ratio r/c and the rotation parameter $V_w/\Omega r$ defining the ratio of the wind velocity to the tangential velocity. The rotation parameter shows the interaction between the axial flow (wind) and the rotational flow induced by the rotor blades. The physical mechanism driving the 3-D effects is in conjunction with the interaction between the wind speed higher than the design velocity and the flow induced by constant-rotational speed rotors. If the rotation parameter is less than unity along the entire span ($V_w/\Omega r < 1$), and for properly twisted blades, the flow is generally attached and nonaffected by it. But the wind turbine blades often operate in deep stall with $V_w/\Omega r > 1$ at the inner part of the span producing both strong centrifugal and Coriolis forces that involve the separation of the boundary layer on the blade. Larger rotation parameters mean enhanced rotational flow that reduces the negative pressure peak from the leading edge and produces leading-edge separation bubbles (not leading-edge stall). On the other hand, the Coriolis forces contribute to stall delay by a favorable chordwise pressure gradient. The occurrence of what is termed inboard stall delay, characterized by an abrupt increase in lift and drag, can be attributed to the sudden suck of air from the separation bubble at the leading edge of the blade that is directed toward the radial direction. Of concern here are the small separation bubbles that form near the leading edge of the inboard sections of the blade, at $r/c = 1$. At extreme inboard locations, separation bubble initiation and aft progression are closely associated with poststall lift force magnitudes that exceed those exhibited by nonrotating blades.

The flow in the vicinity of the leading edge of a blade section subject to leading-edge stall is as sketched in Fig. 1. The laminar boundary layer, extending from the stagnation point over the leading edge, separates just downstream of the point of minimum pressure. Transition to turbulent flow occurs in the free-shear layer a short distance downstream of the separation point. The flow then reattaches to the section surface, with a turbulent boundary layer extending from the reattachment point to the trailing edge. If the r/c ratio is decreased, the bubble becomes slightly shorter and ultimately coalesces in a singular topological entity [1].

Received 25 January 2010; revision received 19 May 2010; accepted for publication 15 June 2010. Copyright © 2010 by the American Institute of Aeronautics and Astronautics, Inc. All rights reserved. Copies of this Note may be made for personal or internal use, on condition that the copier pay the $10.00 per-copy fee to the Copyright Clearance Center, Inc., 222 Rosewood Drive, Danvers, MA 01923; include the code 0021-8669/10 and $10.00 in correspondence with the CCC.

*Senior Researcher, Fluid Dynamics Department, Calea 13 Septembrie Number 13.

The interaction between the viscous and inviscid flows in the vicinity of the bubble is taken into account through a simplified procedure in the sequel.

II. Representation of Flow Elements

A 3-D model has been devised in order to identify the influence of the 3-D and rotational effects on the blade section characteristics. The incompressible 3-D boundary-layer equations are written in integral form in the cylindrical coordinate system (θ, r, z), which rotates with the blade with a constant-rotational speed Ω (Fig. 2). The peripheral is denoted by θ, r denotes the radial (blade spanwise), and z denotes the axial direction.

A. Inviscid Flow

To find the velocity at the airfoil surface in the absence of viscous effects, the reference velocity at a point on a rotating wind turbine blade is

$$U_r = \sqrt{V_w^2 + (\Omega r)^2} \tag{1}$$

where V_w is the wind velocity.

Starting from the idea of Fogarty and Sears [2], an inviscid edge velocity can be calculated as

$$U = \Omega_z r \frac{\partial \phi}{\partial \theta}, \qquad V = \Omega_z(\phi - 2\theta), \qquad W = \Omega_z r \frac{\partial \phi}{\partial z} \tag{2}$$

where $\phi = \phi(\theta, z)$ denotes the two-dimensional (2-D) potential solution that is constant at all radial positions. Thus, the potential edge velocity components can be approached as

$$U_e = U_r U_a, \qquad V_e = 0 \tag{3}$$

where the nondimensional velocity U_a could be obtained by a viscous–inviscid interaction procedure for flow past a 2-D airfoil [3]. However, in order to investigate the leading-edge separation bubble on a stalled blade by means of the boundary-layer method, the velocity U_a is simply considered a linear adverse velocity gradient near the leading edge that, behind the separation, relaxes with the vanishing skin friction. Therefore, the following flow is applied to solve

$$U_e = U_r\left(1 - k\frac{x}{c}\right), \quad \text{for } \frac{x}{c} \le \left(\frac{x}{c}\right)_{\text{sep}} \tag{4}$$

$$U_e \delta_{2x}^{1/(H+2)} = \text{const}, \quad \text{for } \frac{x}{c} \ge \left(\frac{x}{c}\right)_{\text{sep}} \tag{5}$$

where c is the chord length, k is a velocity gradientlike parameter, and δ_{2x} and H are, respectively, the momentum thickness and the boundary-layer shape parameter in the streamwise direction.

Figures 3 and 4 illustrate such chordwise inviscid velocity distributions and the corresponding variations of the peripheral skin-friction coefficient C_{fx} and the boundary-layer shape parameter H, calculated for various values of k, $Re_c = 10^6$, and $r/c = \infty$ (2-D). Laminar separation takes place at $C_{fx} = 0$, and a given value of the shape factor, $H = 3.3$, is used as the criterion for turbulent separation/reattachment. Then, the skin-friction coefficient is truncated for the preceding value. The transition point x_t is the point that corresponds to the minimum skin friction, which, here, is the point of laminar separation.

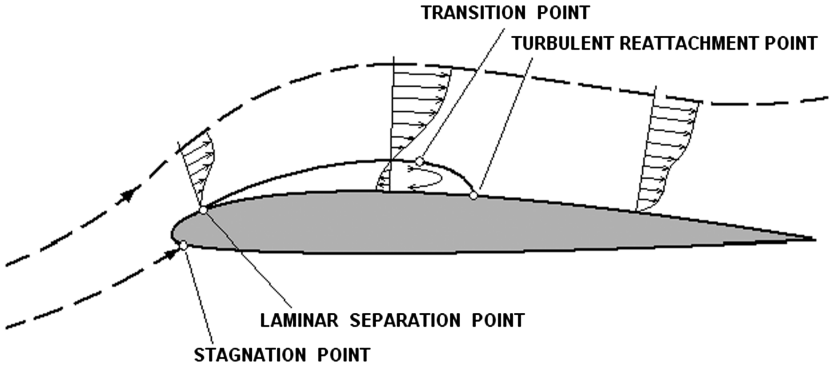

Fig. 1 Flow in the vicinity of a leading-edge bubble.

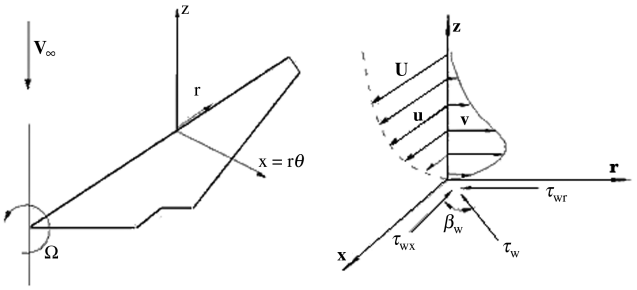

Fig. 2 Cylindrical coordinate system and notation used.

B. Viscous Flow

1. Momentum Integral Equations

The momentum integral equations for the 3-D boundary layer of an incompressible fluid on a rotating blade have been derived by many researchers [1,4,5]. The technique presented in this Note is an extension of the method developed by Dumitrescu and Cardoş for a rotating wind turbine in laminar flow [1]. The new features presented now include the incorporation of a 3-D entrainment equation and the coupling of an inviscid flow near the separation region of the leading edge, with the 3-D momentum integral equations for the boundary-layer calculation.

The coordinate system employed and some of the notations used are shown in Fig. 2, where $x = r\theta$ is the coordinate in the direction of the inviscid streamline at the edge of the boundary layer; r is radial, normal to x; and z is axial, normal to x and the blade surface. The momentum integral equation in the x and r directions in the rotating orthogonal coordinate system is given, respectively, by

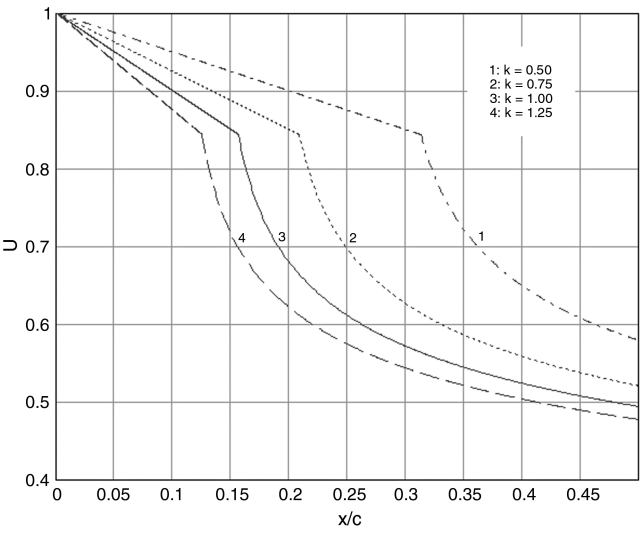

Fig. 3 Chordwise inviscid velocity distribution for various k.

$$\frac{\partial \delta_{2x}}{\partial x} + \frac{1}{U_e}\frac{\partial U_e}{\partial x}(2\delta_{2x} + \delta_{1x}) + \frac{\partial \delta_{2xr}}{\partial r} - \frac{\zeta}{U_e}(2\delta_{2xr} + \delta_{1r}) - 2\frac{\Omega_z}{U_e}\delta_{1r} = \frac{1}{2}C_{fx} \tag{6}$$

and

$$\frac{\partial(\delta_{2xr} + \delta_{1r})}{\partial x} + \frac{2}{U_e}\frac{\partial U_e}{\partial x}(\delta_{2xr} + \delta_{1r}) + \frac{\partial \delta_{2r}}{\partial r} + \frac{1}{U_e}\frac{\partial U_e}{\partial r}(\delta_{2r} + \delta_{1x} + \delta_{2x}) - \frac{\zeta}{U_e}(\delta_{2r} - \delta_{1x} - \delta_{2x}) + 2\frac{\Omega_z}{U_e\delta_{1x}} = \frac{1}{2}C_{fr} \tag{7}$$

where U_e is the inviscid freestream velocity, $\zeta = (\nabla \times \mathbf{V_e})_z = -\frac{1}{r}\frac{\partial}{\partial r}(rU_e)$, and (C_{fx}, C_{fr}) are the skin-friction coefficient components. The usual assumption that the boundary layer is thin compared with the radius of curvature of the blade surface has been made, and the arc length ds in this coordinate system is given by

$$\mathrm{d}s = (\mathrm{d}x^2 + \mathrm{d}z^2 + \mathrm{d}r^2)^{1/2} \tag{8}$$

The various boundary-layer thicknesses are defined as

$$\delta_{2x} = \int_0^\delta \frac{u}{U_e}\left(1 - \frac{u}{U_e}\right)\mathrm{d}z, \qquad \delta_{2xr} = \int_0^\delta \frac{v}{U_e}\left(1 - \frac{u}{U_e}\right)\mathrm{d}z$$
$$\delta_{2r} = -\int_0^\delta \left(\frac{v}{U_e}\right)^2 \mathrm{d}z, \qquad \delta_{1x} = \int_0^\delta \left(1 - \frac{u}{U_e}\right)\mathrm{d}z$$
$$\delta_{1r} = -\int_0^\delta \frac{v}{U_e}\,\mathrm{d}z \tag{9}$$

A power-law-type of velocity profile is assumed for the mainstream velocity profile,

$$\frac{u}{U_e} = \left(\frac{z}{\delta}\right)^{(H-1)/2} \tag{10}$$

where H is the local shape factor.

The assumed crossflow profile is from [4]:

$$\frac{v}{u} = \varepsilon_w\left(1 - \frac{z}{\delta}\right)^2$$

where ε_w is the limiting streamline parameter ($\tan \beta_w$).

Equations (6) and (7) can now be written in terms of the parameters δ_{2x}, ε_w, H, and C_{fx}:

$$\frac{\partial \delta_{2x}}{\partial x} + (2 + H)\delta_{2x}\frac{1}{U_e}\frac{\partial U_e}{\partial x} + \frac{\partial}{\partial r}(L\varepsilon_w\delta_{2x}) - \frac{\zeta}{U_e}(2L + M)\varepsilon_w\delta_{2x} - 2\frac{\Omega_z}{U_e}M\varepsilon_w\delta_{2x} = \frac{1}{2}C_{fx} \tag{11}$$

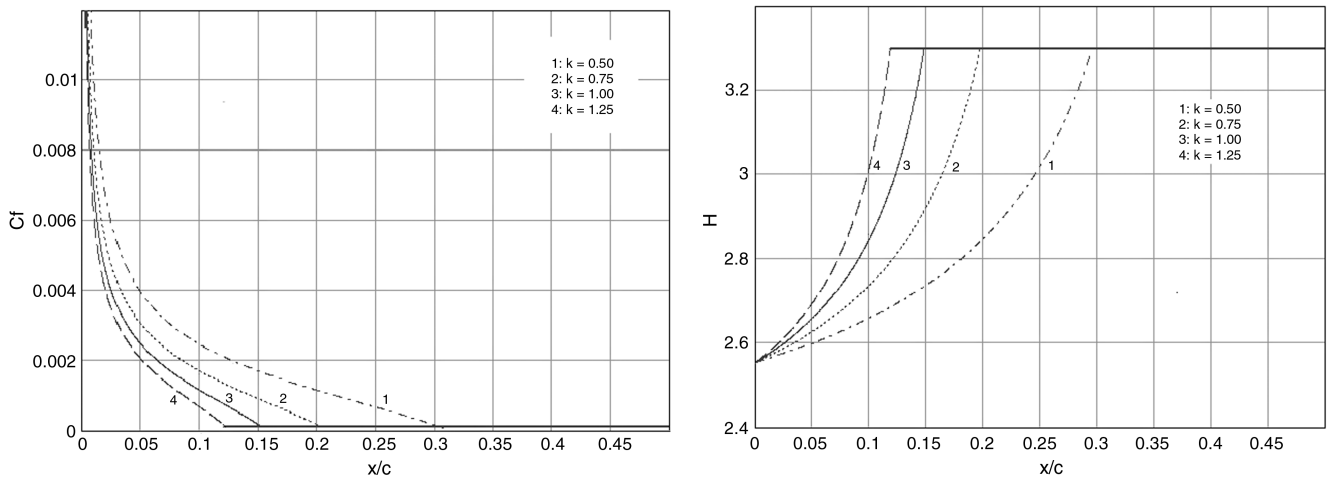

a) b)

Fig. 4 Variation of a) the peripheral skin-friction coefficient and b) the boundary-layer shape parameter.

$$\frac{\partial}{\partial x}[(L+M)\varepsilon_w\delta_{2x}] + \frac{2}{U_e}\frac{\partial U_e}{\partial x}(L+M)\varepsilon_w\delta_{2x} + \frac{\partial}{\partial r}(N\varepsilon_w^2\delta_{2x}) + \frac{1}{U_e}\frac{\partial U_e}{\partial r}(N\varepsilon_w^2 + H + 1)\delta_{2x} - \frac{\zeta}{U_e}(N\varepsilon_w^2 - H - 1)\delta_{2x} + 2\frac{\Omega_z}{U_e}H\delta_{2x} = \frac{1}{2}C_{fx}\varepsilon_w \tag{12}$$

where

$$L = \frac{\delta_{2xr}}{\varepsilon_w\delta_{2x}} = \frac{2(7H+15)}{(H+2)(H+3)(H+5)},$$
$$M = \frac{\delta_{1r}}{\varepsilon_w\delta_{2x}} = -\frac{16H}{(H-1)(H+3)(H+5)}, \tag{13}$$
$$N = \frac{\delta_{2r}}{\varepsilon_w^2\delta_{2x}} = -\frac{24}{(H-1)(H+2)(H+3)(H+4)}$$

The skin-friction relation for flows with pressure gradients and rotation effects is based on the experimental data for a turbulent boundary layer in a rotating channel [5]:

$$C_{fx} = 0.172Re_{\delta_{2x}}^{-0.268}10^{-0.678H}[1 + B_1\sqrt{\varepsilon_w(x - x_t)/c}] \tag{14}$$

This correlation is a modified version of the correlation developed by Ludwieg and Tillmann [6], which includes the effect of rotation. In this relation, B_1 is an empiric constant (a value of 0.52 is used); $Re_{\delta_{2x}}$ is the Reynolds number, based on the streamwise velocity at the edge of the boundary layer and the streamwise momentum thickness δ_{2x}; and x_t is the distance between the leading edge and the transition point along the streamwise direction (the laminar separation point is used).

2. *Closure Model-Entrainment Equation*

The pressure gradients cause large changes in velocity profiles and, consequently, in the shape parameter H. The variation of H cannot be neglected, and an additional equation is required. Out of the available auxiliary equations, only the energy integral equation and the entrainment equation have been suitable for the turbulent boundary layers.

The entrainment equation for the rotor boundary layer in the coordinate system used in this Note can be shown to be

$$\frac{\partial(\delta - \delta_{1x})}{\partial x} + (\delta - \delta_1)\frac{1}{U_e}\frac{\partial U_e}{\partial x} - \frac{\partial\delta_{1r}}{\partial r} + \frac{\zeta}{U_e}\delta_r = C_E \tag{15}$$

where the entrainment coefficient $C_E \equiv [(\partial\delta/\partial x) - (W_e/U_e)]$ is a function of the factor $H_1 = (\delta - \delta_{1x})/\delta_{2x}$. C_E represents the volume flow rate per unit area through the surface $\delta(x, r)$ and is the rate of entrainment of inviscid external flow into the boundary layer.

The entrainment process is a highly complex phenomenon, and an empirical correlation for the entrainment function C_E for 3-D flow is not yet available. Hence, the entrainment function C_E, from Head [7], for 2-D flow is used in the present analysis. The function is given by

$$C_E = 0.0306(H_1 - 3.0)^{-0.653} \tag{16}$$

Also, the similarity solutions show that H_1 is a function of the streamwise boundary-layer shape parameter H. This relationship, which results from a best fit to experimental data [8], is

$$H_1 = 2 + 1.5\left(\frac{1.12}{H-1}\right)^{1.093} + 0.5\left(\frac{H-1}{1.12}\right)^{1.093}, \quad \text{for } H < 4 \tag{17}$$

Then, it is assumed that the variation of the entrainment rate with H_1 follows the same relationship for 3-D flows.

Equation (15) is written in a form similar to Eqs. (11) and (12):

$$\frac{\partial}{\partial x}(\delta_{2x}H_1) + (\delta_{2x}H_1)\frac{1}{U_e}\frac{\partial U_e}{\partial x} - \frac{\partial}{\partial r}(M\varepsilon_w\delta_{2x}) + (M\varepsilon_w\delta_{2x})\frac{\zeta}{U_e} = C_E(H_1) \tag{18}$$

Equations (11), (12), and (18) are to be solved for δ_{2x}, ε_w, and H [H_1 is related to H, Eq. (17)] with the prescribed boundary conditions. At the leading edge, δ_{2x} and ε_w are assumed to be zero, and an initial value of 2.55 (laminar flow) is assumed for H.

3. *Numerical Procedure*

The numerical solution begins from the leading edge of a blade by integrating Eqs. (11) and (12) directly, using the laminar boundary-layer quantities (9) [1] and an inviscid external linear retarded flow [Eq. (4)] that, after the separation, relaxes with the vanishing skin friction [Eq. (5)]. The transition point x_t is chosen to be the laminar separation point, and the shape factor $H = 3.3$ is used to determine the turbulent separation/reattachment point. The initial values for turbulent calculation are determined as a part of the laminar solution for $H = 3.5$. The method of the solution of Eqs. (11), (12), and (18) follows the iterative procedure proposed by Mager [4].

III. Result and Discussions

Although there are a number of computational aerodynamic analyses [9–11], the exact description of the flow in the vicinity of the rotation center is not presently known. Various methods to model the observed effects have been developed [12,13], but the detailed

information of the flow around the rotating airfoil at a high angle of attack near the hub is still rather unclear, and here a new approach could help.

A key element of this analysis is the determination of the separated area on the blade at the leading edge. Four cases of severe adverse gradient flow, at the leading edge, were analyzed using the described method. The results obtained for the chordwise skin-friction coefficient, the boundary-layer shape parameter, and the limiting streamline angle at different small values of nondimensional spanwise distance r/c are used to detect and track boundary-layer separation and reattachment. In the cases under consideration, the patterns of the separation and attachment lines suggest the presence of a conical bubble with high vorticity in the inboard half of the blade and, after the bubble breakdown, a free-shear layer in the outer part of the blade.

Distributions of the chordwise skin-friction coefficient C_{fx} are shown in Fig. 5 at various spanwise distances r/c for the value of the velocity gradient parameter $k = 1$, which corresponds to a severe adverse gradient flow. The points indicated in the figure correspond to laminar separation.

The variations of the chordwise boundary-layer shape parameter are shown in Fig. 6, which notes the turbulent reattachment points according to constant H criterion. The extent of the separated area, defined as the distance between the separation point x_s and the reattachment point x_r, decreases for the decreasing spanwise distance r/c and, at the limit, both points (x_s, x_r) coalesce into a singular point ($C_{fx} = C_{fr} = 0$) with the complex structure (a focus–saddle point combination) [2].

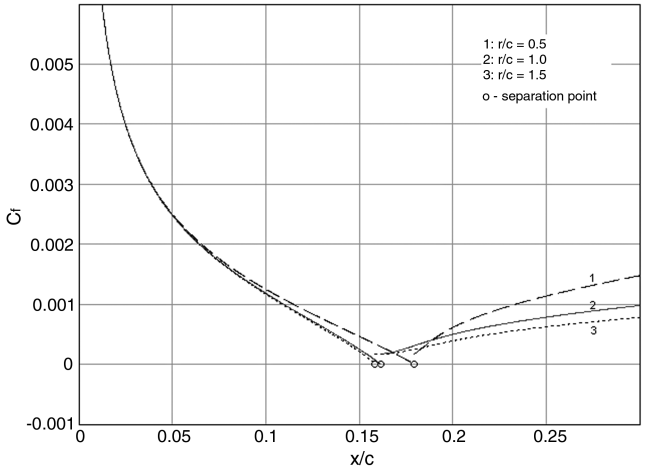

Fig. 5 Chordwise skin-friction coefficient for various ratios.

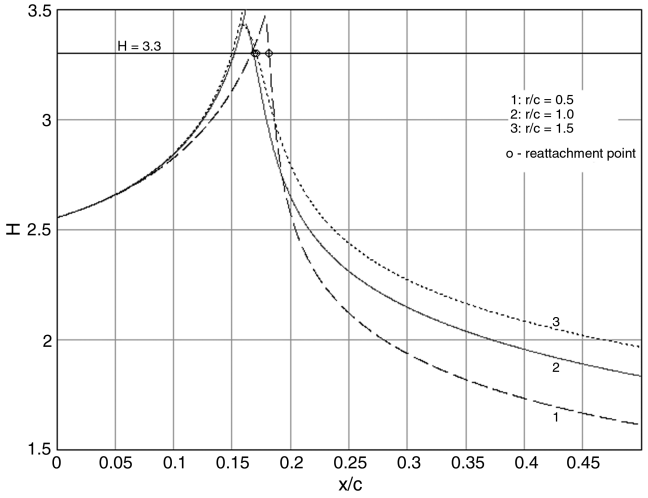

Fig. 6 Chordwise shape factor for various ratios r/c and $k = 1$.

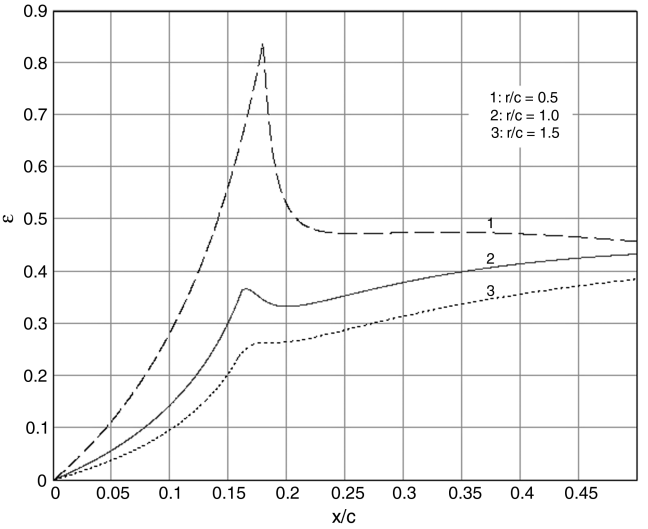

Fig. 7 Chordwise crossflow parameter.

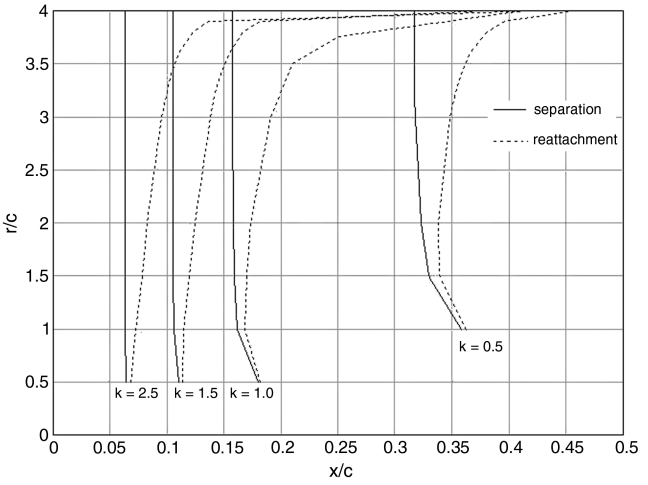

Fig. 8 Predicted separation/reattachment contours.

In Fig. 7, where variations of crossflow angle β_w are shown at varying distances from the rotation axis r/c, an increase of spanwise velocities (and, implicitly, of the Coriolis force) is seen in the separated flow region for decreasing r/c.

Figure 8 shows contours representing rotational leading-edge separation bubbles with high vorticity. The abrupt change in the extent (volume) of the separation bubble observed for all considered cases at approximately $r/c = 4$ (corresponding to midspan) and near the trailing edge could contribute to the bubble breakdown over the suction surface of the blade. The spinning motionlike flow in the separation bubble is thought to represent an inboard standing vortex into the streamwise direction, which decays immediately when its direction is changed. Indirect evidence of such an inboard standing vortex followed by possible a vortex bursting is seen in the circulation plot and local values of the lift and drag coefficients derived based on the Unsteady Aerodynamic Experiment from measurements [14].

IV. Conclusions

The momentum integral technique for the wind turbine blade boundary layer has been extended to include the separated and reattaching shear layer in a leading-edge bubble of a wind turbine blade. Based on the described boundary-layer method, the physical processes that influence the inboard stall-delay phenomenon have been explained, including the onset of the 3-D effects and the increase of the lift coefficients. The major conclusions are as follows:

1) The structure of the separated flow on rotating blades in stall is mainly governed by the three most important parameters: r/c, $V_w/\Omega r$, and Re; r/c, and $V_W/\Omega r$ have a strong effect on the occurrence of the 3-D inboard leading-edge separation bubble (delayed stall), while the quasi-2-D outboard separated flow (leading-edge stall) depends especially on Re.

2) Three entirely different flow patterns can be distinguished: the extreme inboard region ($r/c \leq 1$) of unseparated flow, like the rotating disk in axial flow; the inboard region ($r/c < 4$) of the 3-D flow occupying the leading-edge separation bubbles; and the outboard region ($r/c \geq 4$) of the quasi-2-D separated flow, like the free-shear layer where the flow behind the separation line is redirected to the radial direction.

Besides, there are two interface flows: one between the attached and the leading-edge separated flow holding a singular topological entity and another between the 3-D inboard delayed stall and the quasi-2-D outboard separated flow (in the vicinity of the midspan, $r/c \approx 4$), when the bubble breakdown is produced.

3) The conjectured pattern of skin-friction lines near the root of the blade ($r/c \leq 1.0$) involves singular points with complex topology, namely, a focus–saddle point combination. Physically, this topological structure represents the onset of the leading-edge separation bubble that triggers the 3-D and rotational effects.

4) Accurate predictions of stall and poststall airfoil performance at inboard locations must include the induced effects from the spanwise distribution of proper additional circulation.

References

[1] Dumitrescu, H., and Cardoş, V., "Modelling of Inboard Stall Delay Due to Rotation," *Journal of Physics: Conference Series*, Vol. 75, 2007, Paper 012022.
doi:10.1088/1742-6596/75/1/012022

[2] Fogarty, L. E., and Sears, W. R., "Potential Flow Around a Rotating Advancing Cylindrical Blade," *Journal of the Aeronautical Sciences (Readers' Forum)*, Vol. 17, No. 10, 1950, pp. 599–601.

[3] Drela, M., "XFOIL: An Analysis and Design System for Reynolds Number Aerodynamics," Univ. of Notre Dame, South Bend, IN, June 1989.

[4] Mager, A., "Generalization of Boundary-Layer Momentum-Integral Equations to Three-Dimensional Flows Including Those of Rotating Systems," NACA Rpt. 1067, 1951.

[5] Lakshminarayana, B., and Govindan, T. R., "Analysis of Turbulent Boundary Layer on Cascade and Rotor Blades of Turbomachinery," *AIAA Journal*, Vol. 19, No. 10, 1981, pp. 1333–1341.
doi:10.2514/3.60067

[6] Ludwieg, H., and Tillmann, W., "Untersuchungen über die Wandschubspannung in Turbulenten Reibungsschichten ," *Inginieur-Archiv*, Vol. 17, No. 4, 1949, pp. 288–2990939-1533; also "Investigations of the Wall Shearing Stress in Turbulent Boundary Layers," NACA TM 1285 (in English).
doi:10.1007/BF00538855

[7] Head, M. R., "Entrainment in Turbulent Boundary Layers," British Aeronautical Research Council, Rpt. 3152, Sept. 1958.

[8] Lock, R. C., and Williams, B. R., "Viscous–Inviscid Interactions in External Aerodynamics," *Progress in Aerospace Sciences*, Vol. 24, No. 2, 1987, pp. 51–171.
doi:10.1016/0376-0421(87)90003-0

[9] Johansen, J., and Sorensen, N. N., "Aerofoil Characteristics from 3D CFD Rotor Computations," *Wind Energy*, Vol. 7, No. 4, 2004, pp. 283–294.
doi:10.1002/we.127

[10] Schmitz, S., and Chattot, J. J., "Characterization of Three-Dimensional Effects for the Rotating and Parked NRER Phase VI Wind Turbine," *Journal of Solar Energy Engineering*, Vol. 128, No. 4, Nov. 2006, pp. 445–454.
doi:10.1115/1.2349548

[11] van Rooij, R. P. J. O. M., and Arens, E. A., "Analysis of the Experimental and Computational Flow Characteristics with Respect to the Augmented Lift Phenomenon Caused by Blade Rotation," *Journal of Physics: Conference Series*, Vol. 75, 2007, Paper 012021.
doi:10.1088/1742-6596/75/1/012021

[12] Hu, D., Hua, O., and Du, Z., "A Study on Stall-Delay for Horizontal Axis Wind Turbine Blade," *Renewable Energy*, Vol. 31, No. 6, 2006, pp. 821–836.
doi:10.1016/j.renene.2005.05.002

[13] Xu, G., and Sankar, L. N., "Development of Engineering Aerodynamics Models Using a Viscous Flow Methodology on the NREL Phase VI Rotor," *Wind Energy*, Vol. 5, Nos. 2–3, 2002, pp. 171–183.
doi:10.1002/we.73

[14] Tangler, R., "Insight into Wind Turbine Stall and Post-Stall Aerodynamics," *Wind Energy*, Vol. 7, No. 3, 2004, pp. 247–260.
doi:10.1002/we.122